JOURNAL OF MATERIALS SCIENCE **38** (2003) 1631 – 1643

Processing and mechanical characterization of lightweight polyurethane composites

V. B. CHALIVENDRA, A. SHUKLA*
Dynamic Photomechanics Laboratory, Department of Mechanical Engineering and Applied Mechanics, University of Rhode Island, Kingston, RI 02881, USA
E-mail: shuklaa@egr.uri.edu

A. BOSE
Department of Chemical Engineering, University of Rhode Island, Kingston, RI 02881, USA

V. PARAMESWARAN
Dynamic Photomechanics Laboratory, Department of Mechanical Engineering and Applied Mechanics, University of Rhode Island, Kingston, RI 02881, USA

A simple procedure was established to fabricate polyurethane-cenosphere particulate composite materials. Composites having four different volume fractions of cenospheres (hollow ceramic microspheres) ranging from 10 to 40% in increments of 10% were prepared and their mechanical properties were evaluated. A predictive model to estimate the fracture toughness of the composite was developed. The dynamic constitutive behavior of the composite in compression was investigated using the split Hopkinson pressure bar (SHPB) technique in conjunction with high-speed photography. The results of the material characterization indicated that addition of cenospheres decreased the density of the composite. The quasi-static stiffness, both in tension and compression, and the quasi-static fracture toughness of the composite increased with addition of cenospheres. The high strain rate constitutive behavior of 100% polyurethane showed monotonic stiffening whereas the composite at higher cenosphere volume fractions (40%) exhibited a stiffening-softening-stiffening behavior. Scanning Electron Microscopy (SEM) studies were also carried out to determine the failure mechanisms of the composite.

1. Introduction

Polyurethane composites, originally developed as an alternative material to rubber composites, have superior mechanical properties. Considerable work has been done on fabrication and quasi-static evaluation of various types of polyurethane composite materials. Yilzmer *et al*. [1] studied the mechanical-dilatational behavior of glass-bead-filled polyurethane as a function of filler content, particle size, and surface treatment of the filler. Chehab *et al*. [2] conducted an experimental investigation of dynamic mechanical relaxation behavior and tensile stress-strain behavior of polyurethane/mica composite as a function of filler concentration and surface area of the filler. Rozman *et al*. [3] studied the effect of adding oil palm empty fruit bunch to polyurethane on tensile properties. Recently, Torro-Palau *et al*. [4] studied the effect of four different types of silica in thermoplastic polyurethane on the rheological, mechanical and adhesion properties of the composite. Molnar *et al*. [5] investigated the impact resistance and fracture characteristics of multi-component polypropylene particulate composites. Recently, Cardoso *et al*. [6] used ceramic-microballons as reinforcements in thermosetting polyester resin to develop lightweight composites. They investigated the effect of particle size and particle surface treatment on constitutive properties of these composites. The effect of particle size and volume fraction on the fracture toughness of polyester resin, reinforced with micrometer and nanometer sized aluminum particles, was investigated by Singh *et al*. [7].

Literature also reveals that there has been extensive work done on dynamic characterization of various types of elastomers. Very recently, Sharma *et al*. [8] used high-speed photography along with the split Hopkinson pressure bar (SHPB) technique to study the dynamic constitutive behavior of soft materials including polyurethane. Chen *et al*. [9] also used SHPB along with high speed imaging to investigate the dynamic constitute behavior of silicon rubber. However, fabrication and characterization of lightweight polyurethane elastomer based composite materials are not yet reported. This paper discusses the fabrication and detailed quasi-static and dynamic mechanical characterization

*Author to whom all correspondence should be addressed.

of lightweight polyurethane-cenosphere particulate composites.

A simple procedure was established to fabricate consistent quality composites. Composites having volume fractions of cenospheres ranging from 10 to 40% in increments of 10% were prepared. A detailed quasi-static characterization of constitutive behavior and fracture toughness was performed to identify the effect of particle strengthening on Young's modulus, tensile strength, % elongation at break and fracture toughness. High-speed photography in conjunction with the split Hopkinson pressure bar (SHPB) technique was used to characterize the dynamic constitutive behavior in compression at two different strain rates. A fractographic analysis of fractured specimens was also performed to identify the failure mechanisms.

2. Fabrication procedure

The thermoset and cross-linked elastomer, polyurethane, used as matrix in this study consisted of two parts: Part A (resin) and Part B (Hardener). The specific gravity of both parts is 1.16 and the mix ratio was 1:1. The basic rationale in using this type of urethane is that it is flexible and easy to use. Due these characteristics, this polyurethane has many naval applications such as vibration isolation and shock absorption. The viscosity of this urethane is very low and this makes it suitable for mixing the particles up to 40% volume fraction without air entrapment. *Cenospheres* [10–12] were used as the particle reinforcement. Cenospheres are silica-alumina micro spheres ranging from 10 to 300 μm in diameter. These hollow spheres are a by-product of the fly ash, obtained from coal-fired power plants. Since fly ash is a waste product any use of it is beneficial for the environment. The physical and chemical properties of the cenospheres used in this study are provided in Table I.

As polyurethane is a soft material, it is difficult to make the test specimens by machining. Suitable molds were therefore made to cast the standard test specimens required for characterization of the composite. A silicone blend mold-releasing agent was applied to the molds for easy removal of specimens from the mold. As the polymerization process of polyurethane is very sensitive to moisture, cenospheres were first air-dried at 100°C for an hour. Since part A is highly viscous compared to part B, the entire cenospheres were added to part B first. Part A, and part B with particles were degassed separately to remove the entrapped air. Both parts were then mixed thoroughly and degassed again to remove any air entrapped during mixing. The mix was then poured into suitable molds to make the desired test specimens. Proper care was taken not to induce any air bubbles while pouring the mix into the molds. The reason for degassing before mixing both parts was to reduce the degassing time after mixing, as polyurethane has a short gelation time of 25 minutes. The specimens were cured at room temperature for 24 hours in the mold. Subsequently they were taken out from the mold and cured at room temperature for 10 days to achieve complete polymerization.

TABLE I Properties of cenospheres[a]

Physical properties		Chemical composition (%)	
Specific gravity	0.67	Silica, SiO_2	64.4
Bulk density	375 kg/m^3	Alumina, Al_2O_3	29.4
Size range	10–300 μm	Iron oxide, Fe_2O_3	4.3
Mean size	127 μm	Titania, TiO_2	1.0
Wall thickness	0.1 diameter	Organic matter	0.9

[a]Product information for LV01-SG from Sphere Services Inc.

TABLE II Mass density of the composite for various volume fractions of cenospheres

Volume fraction of cenospheres	Mass density of the composite (kg/m^3)
0	1090
10	1050
20	990
30	950
40	900

3. Mass density characterization

Mass density of the composite was determined for all volume fractions. Table II shows the variation of mass density as a function of cenosphere volume fraction. Owing to the low specific gravity of cenospheres, the density of the composite decreases by 20% as the volume fraction of cenospheres is increased to 40%. The composites having cenosphere volume fraction of 20% and more float in water.

4. Quasi-static characterization

4.1. Constitutive response in tension

Tensile tests were carried out according to ASTM D412 test method using an Instron material testing system. Five different samples of each volume fraction were tested. Constitutive behavior and various tensile properties such as Young's modulus, tensile strength, specific tensile strength and % elongation at break were determined for the four volume fractions and for 100% polyurethane. Fig. 1 shows typical stress-strain plots of the composites as a function of volume fraction of cenospheres. These plots show an initial linear region followed by a nonlinear region. The extent of the linear portion of the curve increases as the volume fraction of the cenospheres increases. This is due to the reinforcement effect provided by the cenospheres. It can also be observed from the plot that the composites at higher volume fractions, exhibit significant softening in the nonlinear region of the stress-strain curve. This is attributed to the debonding of the matrix from the particles, widely known as dewetting. The effect of dewetting is predominant at higher volume fractions.

The Young's modulus of the composites determined from the initial linear portion of the stress-strain plot is shown in Fig. 2. Addition of cenospheres increases the stiffness of the composite. The Young's modulus of the composite having 40% volume fraction of cenospheres is five times that of polyurethane. The increase in Young's modulus with addition of cenospheres is due to the restriction imposed by the relatively rigid

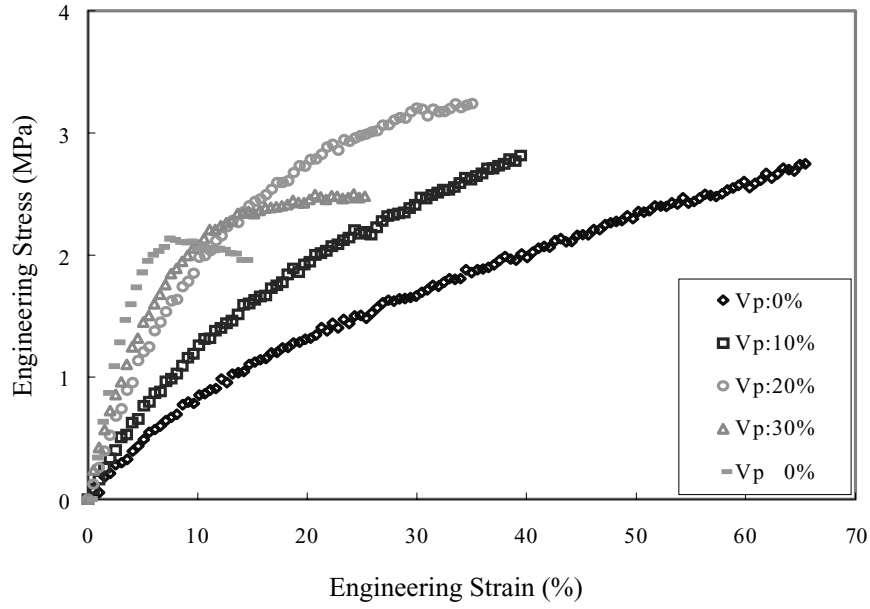

Figure 1 Quasi-static tensile constitutive behavior as a function of volume fraction (V_p) of cenospheres.

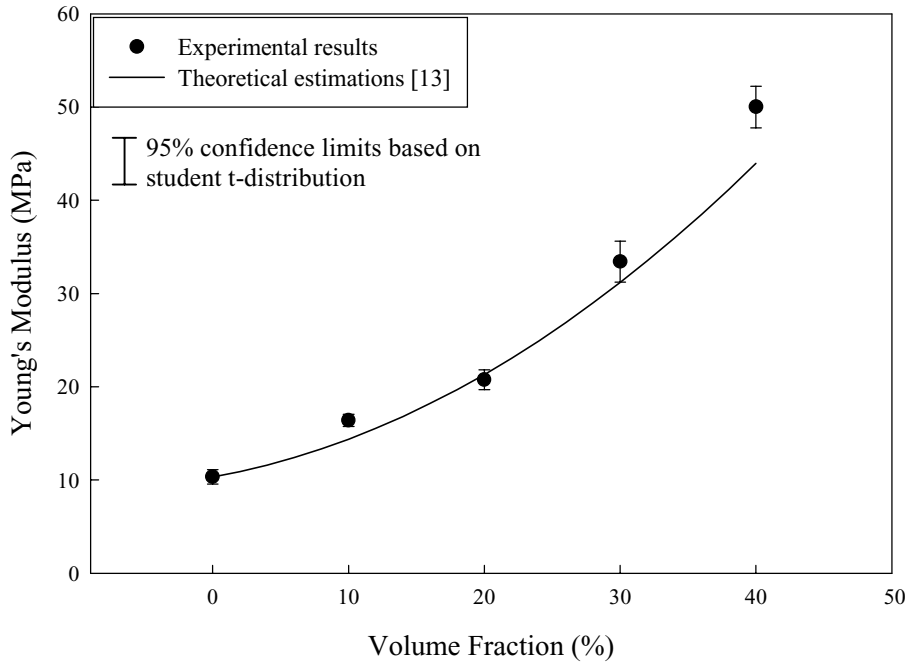

Figure 2 Effect of particle reinforcement on tensile Young's modulus.

cenospheres on deformation of the matrix. These Young's modulus values were compared with estimates obtained using the theoretical model proposed by Guth [13], given in Equation 1

$$E_c = E_m \left(1 + 2.5\ V_p + 14.1\ V_p^2\right) \qquad (1)$$

where V_p is volume fraction of the particles in the composite and E_c and E_m are the Young's modulus of composite and matrix respectively. Though this model is typically used for lower volume fractions, the predictions compare well with those obtained using other models up to 30% filler volume fractions as shown by Bergstrom [14]. As shown in Fig. 2, the estimates determined using Equation 1 have a maximum deviation of 12% from experimental data. The deviation at higher volume fractions occurs because the model does not consider multiple particle interactions.

The effect of addition of cenospheres on tensile strength is shown in Fig. 3. The tensile strength increases up to 20% volume fraction of cenospheres and decreases with further addition of cenospheres. There are two major competing phenomena affecting the tensile strength. The increase in the tensile strength of the composite is due to load sharing by the cenospheres. At the same time, introduction of these rigid particles in a soft matrix causes localized stress intensification. As the volume fraction of cenospheres increases, the stress concentration increases. These high stresses initiate debonding or dewetting of the matrix from the particles. Once dewetting occurs, load sharing by the cenospheres decreases. The debonded region acts essentially as a void and reduces the tensile strength. The effect of dewetting on tensile strength is predominant only at higher volume fractions. Yilmazer and Farris [1]

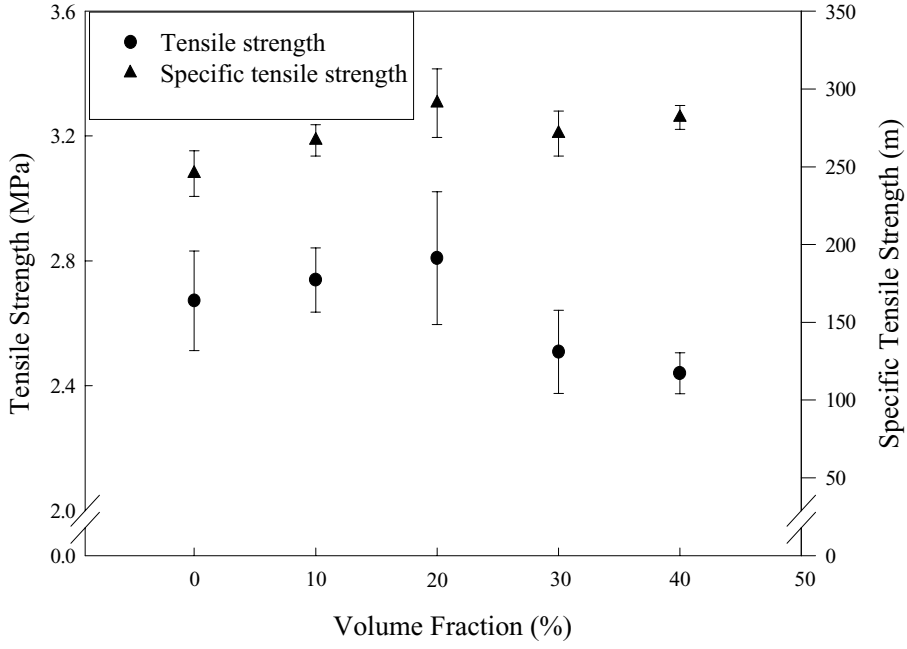

Figure 3 Tensile strength and specific tensile strength as a function of volume fraction of cenospheres.

also observed a similar trend for tensile strength with the addition of rigid particles to an elastomer matrix. The variation of the specific tensile strength (ratio of tensile strength to weight density) as a function of the volume fraction of cenospheres, shown in Fig. 3 indicates that the specific tensile strength of composite is more than that of polyurethane for all volume fractions.

An SEM image of the failure surface for a composite containing 40% cenospheres is shown in Fig. 4. The clean surfaces of the unbroken cenospheres and impressions of the pop-outs of cenospheres indicate that the primary failure mode is matrix dewetting and matrix failure. The void between the matrix and cenospheres shown in the micrograph is due to partial dewetting.

Fig. 5 shows the effect of particle reinforcement on percentage elongation at break. The percentage elongation at break decreases with addition of cenospheres. As mentioned earlier, the failure of the composite was primarily through matrix failure and dewetting. Thus,

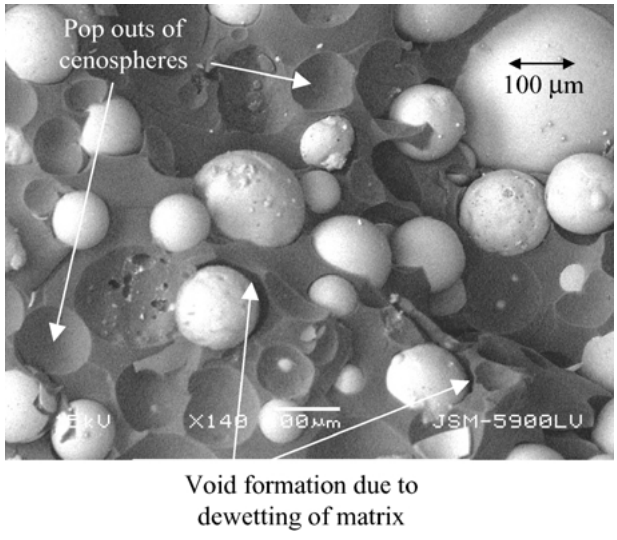

Figure 4 SEM image of tensile fracture surface composite having 40% volume fraction of cenospheres.

for the composite to fail, the local strains in the matrix should reach the failure strain of polyurethane. Addition of cenospheres decreases the composite failure strain because of two reasons. First, the overall stiffenening and the load sharing provided by the rigid cenospheres causes the localized matrix strain to reach the failure strain of polyurethane at relatively low overall composite strains. Additionally, as the cenosphere volume fraction increases, dewetting (prior to failure) and the associated effetcs of voids become predominant leading to a further reduction in the failure strain of the composite. For all the volume fractions, the failed test specimens did not indicate any permanent deformation.

4.2. Constitutive response in compression

Five different samples of each volume fraction were tested for compression behavior according to ASTM D575 test method. Specimens were loaded up to 50% axial engineering strain. Quasi-static constitutive behavior and Young's modulus as a function of cenosphere volume fraction were determined. Fig. 6 shows typical engineering stress-strain behavior of the composite as a function of volume fraction of cenospheres. The Young's modulus was determined by considering the initial linear portion up to 0.4% engineering strain as shown in Fig. 7. The Young's modulus as a function of volume fraction of cenospheres, shown in Fig. 8, indicates that the estimates obtained using Guth's [13] predictive model given in Equation 1 have a maximum deviation of 8% from experimental results. The increase of Young's modulus is due to the constraint imposed by the cenospheres on matrix deformation. The softening behavior at higher strain values in the stress-strain response for 40% volume fraction is attributed to the debonding of cenospheres, which is predominant at higher volume fraction. Unlike the tensile specimens, the specimens tested in compression did not recover their initial dimensions upon unloading and permanent deformations of 3 to 5% were measured. It was also

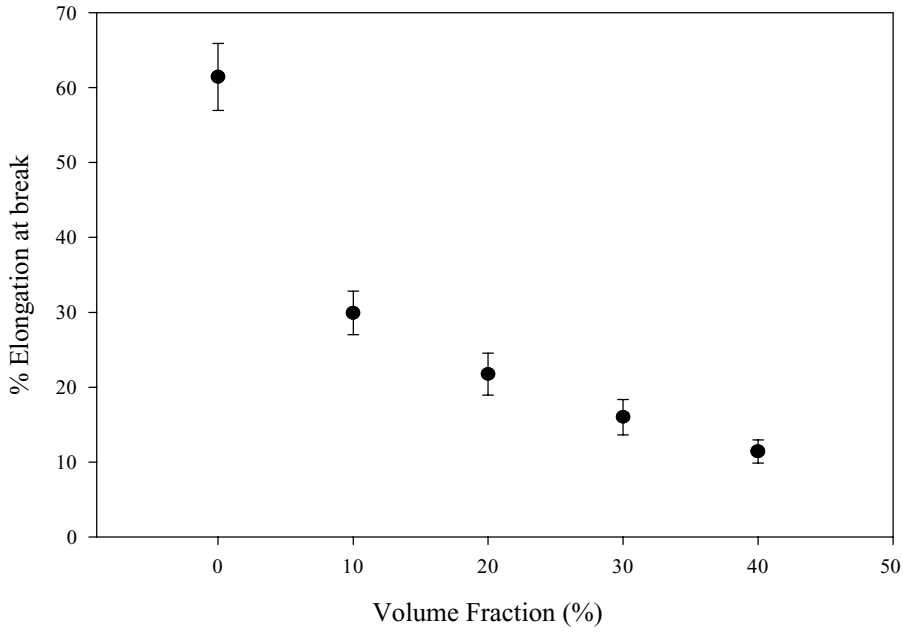

Figure 5 Effect of particle reinforcement on percentage elongation at break.

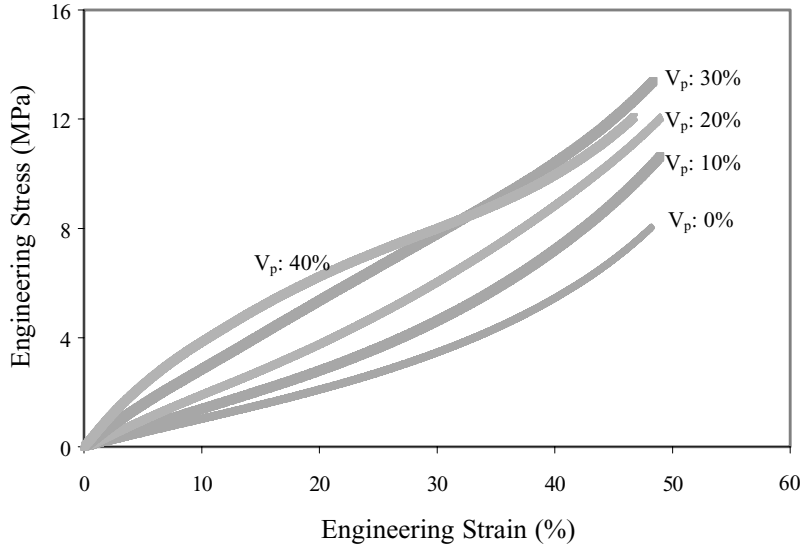

Figure 6 Quasi-static constitutive behavior under compression as a function of volume fraction (V_p).

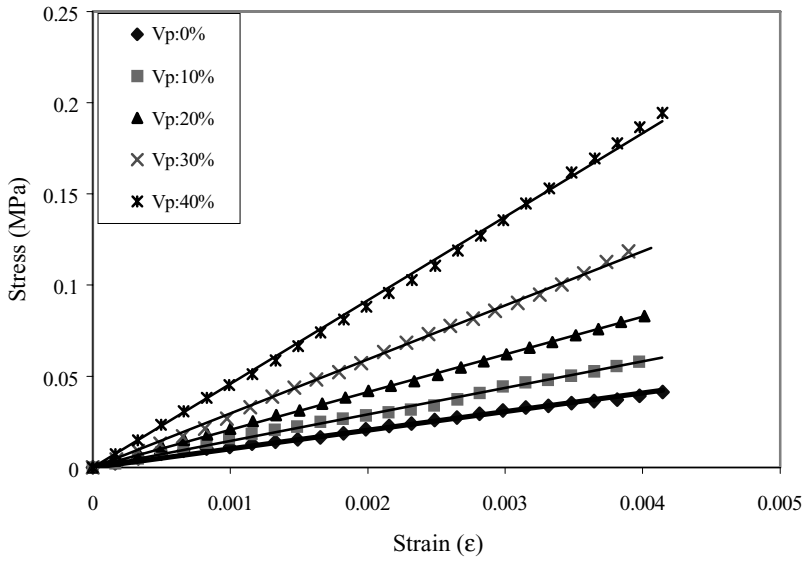

Figure 7 Linear portion of the quasi-static constitutive behavior under compression as a function of volume fraction (V_p). (The coefficient of regression (R^2) for all trend lines is 0.99).

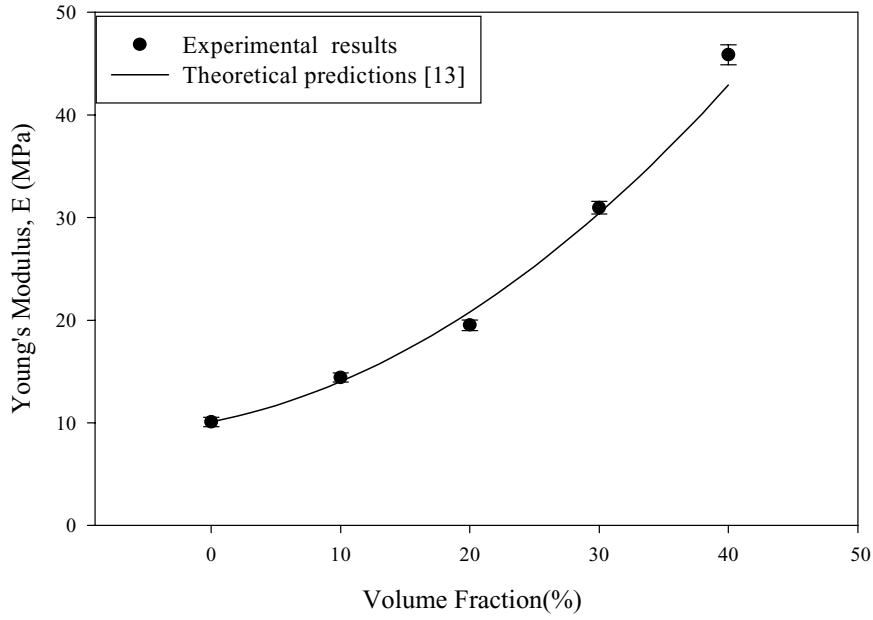

Figure 8 Effect of particle reinforcement on Young's modulus under quasi-static compression.

noticed that all the specimens were intact without any cracking.

4.3. Fracture characterization

4.3.1. Experimental determination of fracture toughness

Quasi-static fracture toughness was determined using single-edge notch tension (SENT) specimen configuration shown in Fig. 9. A fine razor blade was used to make an initial crack of root radius 20 μm, which is six times smaller than the mean diameter of cenospheres. Fig. 10 represents the load-load point displacement plots as a function of volume fraction for the crack length used in this study. It was observed that for all volume fractions the load-displacement plot is linear up to the fracture initiation load. Hence linear elastic fracture mechanics was used to determine the quasi-static fracture toughness. Five samples of each volume fraction were tested to obtain the fracture toughness (K_{IC}) using an Instron material testing system. Fig. 11 shows the effect of cenosphere reinforcement on fracture toughness. The fracture toughness of the composite having 40% volume fraction of cenospheres is twice that of polyurethane. There are three reasons for the increase in fracture toughness. (1) The reinforcement of matrix increases load carrying capacity of the composite, thus increasing the fracture initiation load and fracture toughness. (2) Presence of the higher stresses near the crack tip causes dewetting, which results in blunting of the crack. Additionally, dewetting in the fracture process zone around the crack tip can result in some stress relief before the onset of crack propagation. (3) The cenospheres that have not debonded from the matrix could also increase the fracture initiation load through crack bridging and crack pinning mechanisms in the fracture process zone.

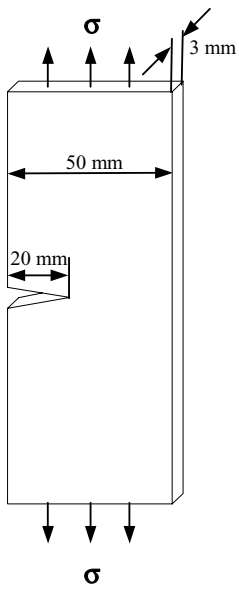

Figure 9 Single edge notch specimen for measuring fracture toughness.

4.3.2. Predictive model to estimate fracture toughness

There have been extensive number of both theoretical and empirical models developed to determine Young's modulus and stress-strain behavior of elastomer matrix particulate composite materials, however, there is no predictive model available in the literature to estimate fracture toughness of the elastomer matrix particulate composite. Recently, El-Hadek and Trippur [15] developed a theoretical model for estimating tensile strength of porous materials based on strain energy concept. Based on the same theory, an attempt has been made in this paper to develop a theoretical model to estimate fracture toughness of elastomer matrix rigid particulate composite material. Fig. 12 shows a strip of a particulate composite material of thickness t, width b and length L. There are two basic assumptions used in this model: (1) the particles are rigid and they do not deform and (2) the overall strain energy of the composite is equal to the strain energy stored in the matrix. By considering the loading of the strip as a plane strain

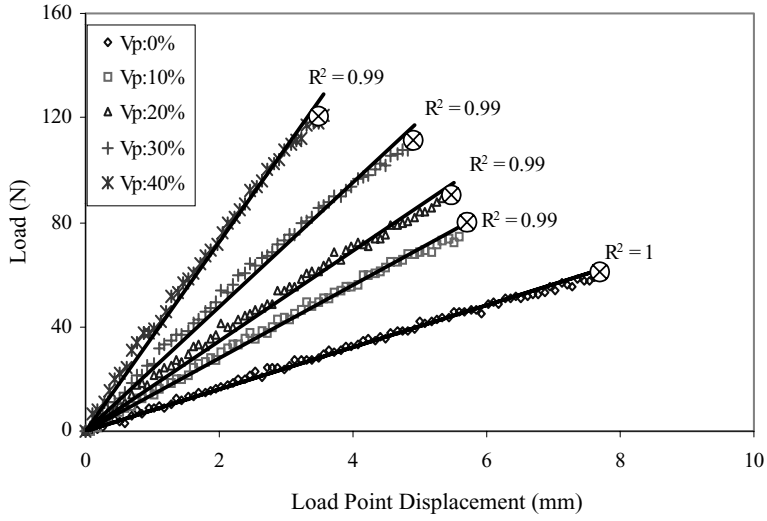

Figure 10 Load-load point displacement plots of SENT specimen for various volume fractions.

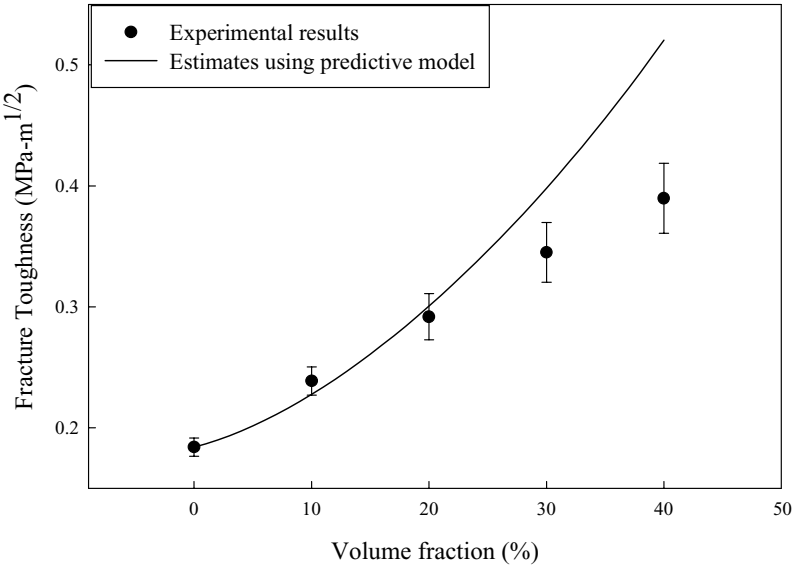

Figure 11 Effect of particle reinforcement on fracture toughness.

problem, for linear elastic material behavior, the strain energy can be written as

$$AL\left(\frac{1}{2}\sigma_c\varepsilon_c\right) = A'L\left\langle\frac{1}{2}\sigma_x\varepsilon_x + \frac{1}{2}\sigma_y\varepsilon_y + \frac{1}{2}\tau_{xy}\gamma_{xy}\right\rangle_m \quad (2)$$

where A is nominal cross-sectional area of the composite and A' is average reduced cross-sectional area of the matrix excluding the particle areas normal to the far-field stress applied in the x-direction. σ_c and ε_c are the stress and strain in the composite in the direction of loading. The contribution to the strain energy from the second and third terms in the right hand side of Equation 2 is much smaller compared to that of the first term and, hence can be neglected. A simple

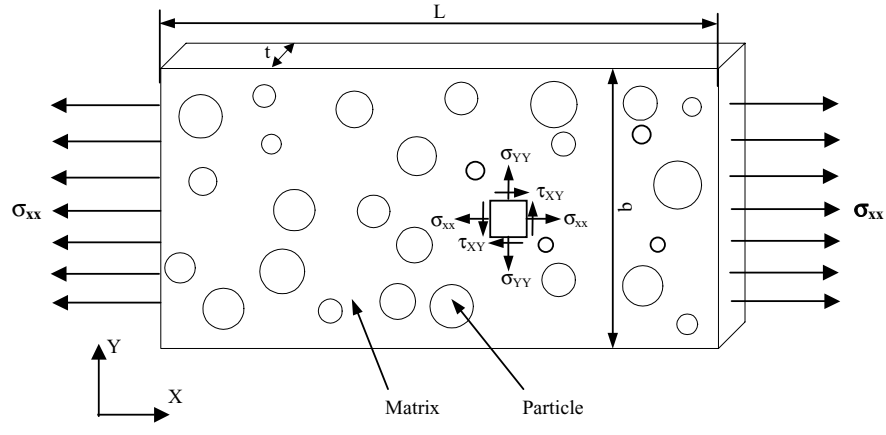

Figure 12 A finite strip of particulate composite under uniaxial tension.

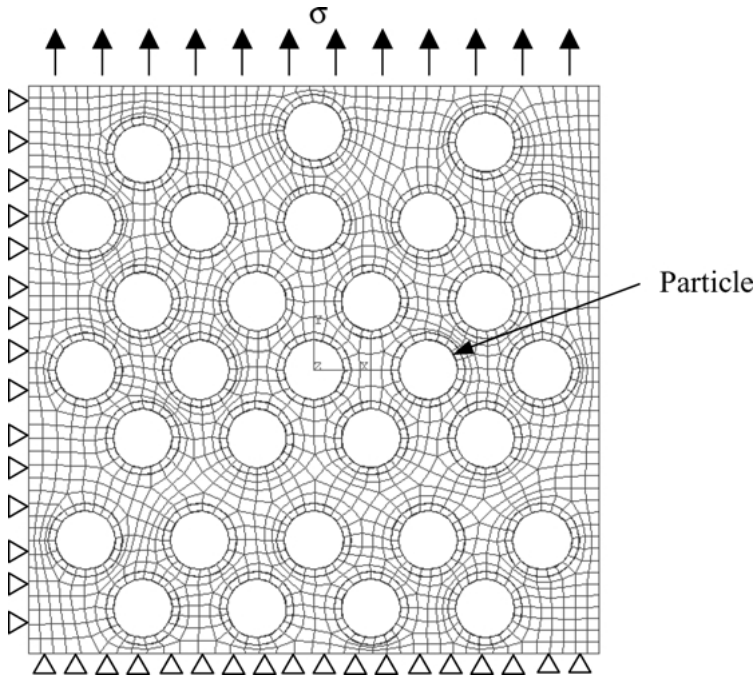

Figure 13 The finite elements mesh for 40% volume fraction of cenospheres, where the element size is 20 μm.

elasto-static finite element analysis was performed using the finite element analysis program, ABAQUS-Standard, to verify this approximation. The model used for this verification is shown in Fig. 13. Due to symmetry, only a fourth of the strip was used in the analysis. Two-dimensional plane strain annular cylindrical particles were considered instead of three-dimensional hollow spherical particles for simplicity. The dimensions of the annular particles used in this study are: outside diameter of 130 μm and thickness of 13 μm (analogous to the dimensions of cenospheres). The particles have a higher Young's modulus of 220 GPa, as determined by Rohatgi and Guo [16]. It was observed from the results of finite element analysis that both normal and shear strains of the particles are very small compared to those of the matrix. Hence the two assumptions made in the predictive model are valid.

A ratio of the strain energy component ($U' = \frac{1}{2}\sigma_x\varepsilon_x$) to the total strain energy ($U = \frac{1}{2}(\sigma_x\varepsilon_x + \sigma_y\varepsilon_y + \sigma_{xy}\varepsilon_{xy})$) was computed for four different volume fractions of particles ranging from 10 to 40% in increments of 10%. The results showed that U'/U is in the range of 0.96–0.88 for the volume fractions (10 to 40%) of particles used.

The simplified Equation 2 can now be written as,

$$AL\left(\frac{1}{2}\sigma_c\varepsilon_c\right) = A'L\left\langle\frac{1}{2}\sigma_x\varepsilon_x\right\rangle_m = A'L\left(\frac{1}{2}\langle\sigma_m\rangle\langle\varepsilon_m\rangle\right) \tag{3}$$

where $\langle\sigma_m\rangle$, $\langle\varepsilon_m\rangle$ are the average stress and strain in the matrix in the direction of loading.

Considering one dimensional stress distribution and linear elasticity, Equation 3 can be written as below,

$$\sigma_c\left(\frac{\sigma_c}{E_c}\right) = \frac{(A'L)}{(AL)}\,\sigma_m\left(\frac{\sigma_m}{E_m}\right) \tag{4}$$

From Equation 4 the stress in the composite can be related to the stress in the matrix as

$$\sigma_c = \sqrt{1 - V_p}\sqrt{\frac{E_c}{E_m}}\,\sigma_m \tag{5}$$

where V_p is the volume fraction of the particles in the composite and E_c andE_m are the Young's modulus of the composite and matrix respectively. From Equation 5, the failure stress of the composite can be determined by knowing the failure stress of the matrix using the constant parameters V_p, E_c and E_m. Equation 5 can be further represented in terms of the critical fracture load (P_c) as shown below.

$$P_c = \frac{A_c}{A_m}\sqrt{1 - V_p}\sqrt{\frac{E_c}{E_m}}\;P_m \tag{6}$$

where A_c and A_m are the nominal cross-sectional areas of the composite and matrix respectively.

The fracture toughness $(K_I)_c$ of the finite SENT geometry [17] can be determined by using the relation.

$$(K_I)_c = \frac{P_c}{t\sqrt{w}}\,f\left(\frac{a}{w}\right) \tag{7}$$

where t, w, a are thickness, width and crack length of the specimen respectively.

By considering the critical load obtained in Equation 6 as the critical load at which fracture occurs and substituting Equation 6 in Equation 7, gives

$$(K_I)_c = \frac{A_c}{A_m}\sqrt{1 - V_p}\sqrt{\frac{E_c}{E_m}}\;\frac{P_m}{t\sqrt{w}}\,f\left(\frac{a}{w}\right) \tag{8}$$

where A_m/A_c is the matrix fraction of the composite for unit length, which is $(1 - V_p)$.

The above equation can be simplified to represent the fracture toughness of the composite in terms of fracture toughness of the matrix $(K_I)_m$.

$$(K_I)_c = \frac{1}{\sqrt{1 - V_p}} \sqrt{\frac{E_c}{E_m}} \, (K_I)_m \tag{9}$$

4.3.3. Comparison of experimental results with estimates of predictive model

A comparison of the fracture toughness estimated by Equation 9 with those obtained from the experiments shown in Fig. 11 indicates that the estimates of predictive model matches well with the experimental results up to 20% volume fraction of cenospheres. The predictive model over estimates the fracture toughness for volume fractions beyond 20%. The deviation of the model estimates from experimental results beyond 20% volume fraction is primarily due to several reasons. First, E_c itself has a large error bar ±5% at higher volume fractions introducing an error in the fracture toughness estimates. Second, ignoring the second and third terms in the strain energy Equation 2 and assuming one dimensional stress state in Equation 3 also introduce an error in the estimates.

5. Dynamic characterization

5.1. Experimental procedure

The experimental setup consisting of SHPB and high-speed imaging system shown in Fig. 14 was used to study the dynamic constitutive behavior. The SHPB consists of a striker bar, an incident bar and a transmission bar, all made of Aluminum 7075-T651. The specimen (6 mm diameter and 3 mm thickness) was placed between the incident and transmission bars. To minimize frictional effects, a thin layer of molybdenum disulfide lubricant was applied between the specimen and the contacting bar end faces. On the impact surface of incident bar, two layers of paper (pulse shaper) were attached with a thin layer of vacuum grease. This filters out any high-frequency components in the incident pulse. When the striker bar impacts the incident bar, an elastic compressive stress pulse, referred as incident pulse, is generated and propagates along the incident bar towards the specimen. When the incident pulse reaches the specimen, part of the pulse is reflected back into the incident bar due to the impedance mismatch at the bar-specimen interface. The remaining part of the pulse is transmitted into the specimen and, eventually, into the transmission bar. Axial strain gages mounted on the surface of the incident and transmission bars provide time-resolved measures of the elastic strain pulses in the bars. A LeCroy model 6810 data acquisition module was used to acquire the data. Two different strain rates were achieved by varying the impact velocity. Using one-dimensional wave theory [18], the stress (σ_s) and strain (ε_s) histories in the specimen can be generated from the reflected and transmitted strains $(\varepsilon_r, \varepsilon_t)$ as

$$\begin{aligned} \varepsilon_s &= \frac{-2c_b}{l_s} \int_0^t \varepsilon_r(t) \, \mathrm{d}t \\ c_b &= \sqrt{\frac{E_b}{\rho_b}} \\ \sigma_s(t) &= E_b \frac{A_b}{A_s} \varepsilon_t(t) \end{aligned} \tag{10}$$

where, l_s is the specimen length and c_b is the wave speed in the bar material. A_b and A_s are the cross-sectional areas of the bar and specimen respectively. E_b and ρ_b are the Young's modulus and density of the bar material respectively.

An Imacon-200 high-speed imaging system was used to capture real-time strains of material deformation under dynamic loading. This camera is capable of taking 16 pictures at a framing rate as high as 200 million frames/sec with exposure times as low as 5 ns. The incident pulse was used to trigger both the data acquisition system and the camera. Since the incident pulse takes 110 μs to reach the specimen, an initial delay of the same duration was set in the camera to start capturing the real time deformation of the specimen. All the images were taken with an inter-frame time of 10 μs and exposure time of 250 ns.

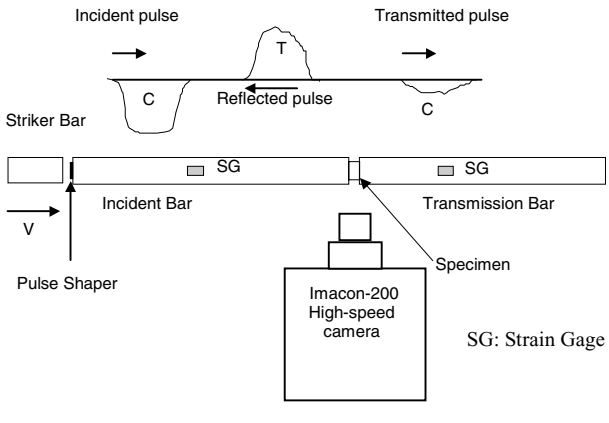

Figure 14 Experimental setup used for dynamic characterization.

5.2. Experimental results

5.2.1. Dynamic constitutive behavior

The dynamic constitutive behavior was determined at two different strain rates 3000/s and 5000/s. Fig. 15 shows typical incident, reflected and transmitted strain pulses from an experiment for polyurethane-cenosphere composite. The reflected pulse was used to compute the axial strain history, and the transmitted pulse was used to compute the stress history in the specimen using Equation 10. The true stress-strain response at an average strain rate of 5000/s is shown in Fig. 16 for all volume fractions. The stress-strain plot for higher volume fractions (30 and 40% cenospheres) exhibits three regions. In the initial region (up to 10% strain) the stiffness is considerably higher than that of polyurethane. In the second region (10 to 40% strain), the material softens as indicated by the reducing slope of the stress strain curve (which eventually becomes close to zero for 40% volume fraction). In the third region (above 40% strains), the material regains some of the stiffness and the slope of this portion of the curve approaches that of the polyurethane stress-strain curve. At higher volume fractions, after reaching a critical load, dewetting of the matrix from the cenospheres happens

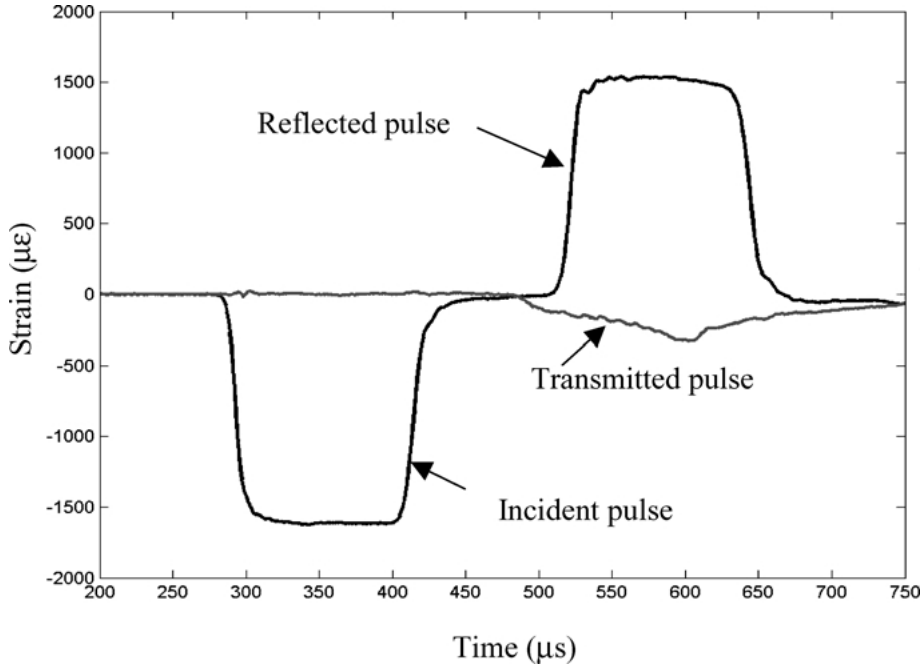

Figure 15 Typical strain-time records for polyurethane-cenosphere composite.

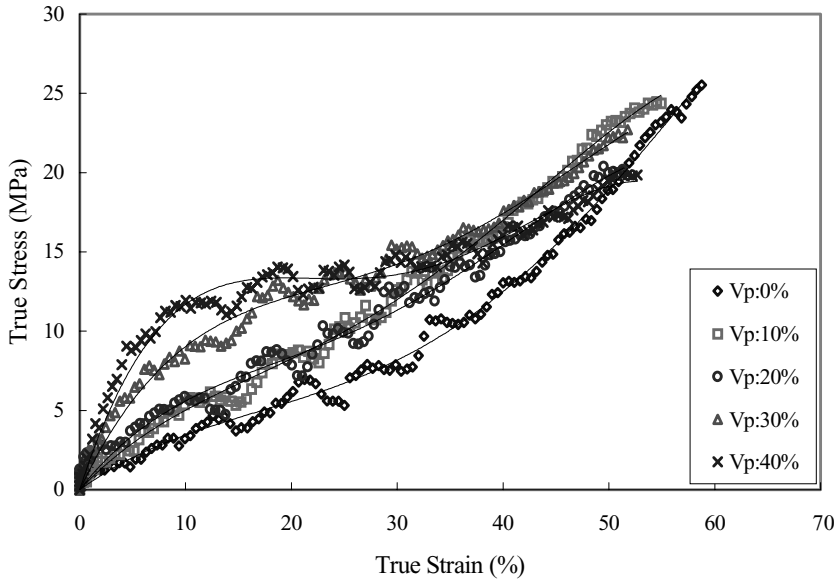

Figure 16 True stress-strain behavior as a function of volume fraction (V_p) of cenospheres for an average strain rate of 5000/s.

spontaneously in the radial direction. This relaxes the constraint on matrix deformation altogether, leading to the softening behavior. However, as the specimen deforms further, the cenospheres will continue to share load by localized direct contact, leading to regaining some of the stiffness.

Fig. 17 shows the true stress-strain behavior as a function of strain rate for polyurethane. It can be seen that there is significant difference between the quasi-static and dynamic constitutive behaviors, indicating that polyurethane by itself is highly rate sensitive. However, the two high strain rate responses are very close to each other. The quasi-static and dynamic response for 40% cenospheres, shown in Fig. 18, indicates that, there is again a dramatic difference between the quasi-static and dynamic constitutive behaviors. Unlike the dynamic response of polyurethane (see Fig. 17), the response of the composite having 40% volume fraction of cenospheres at the two high strain rates do not fall on each other especially in the initial region. In this initial region, the composite stiffness increases with strain rate. The two factors responsible for the increase of stiffness with strain rate at higher volume fractions are 1) rate sensitivity of the matrix and 2) constraint imposed by the cenospheres. The constraint imposed by the cenospheres increases with strain rate as the cenospheres have less time available to pack themselves during the deformation process.

Post test inspection of the samples indicated multiple cracks in the 30% and 40% volume fraction samples, whereas no such damage was observed for the other volume fractions. The damaged test specimens were inspected in an optical microscope for delamination and crushing of cenospheres. There was evidence of debonding of spheres from the matrix, however no broken or crushed spheres were noticed.

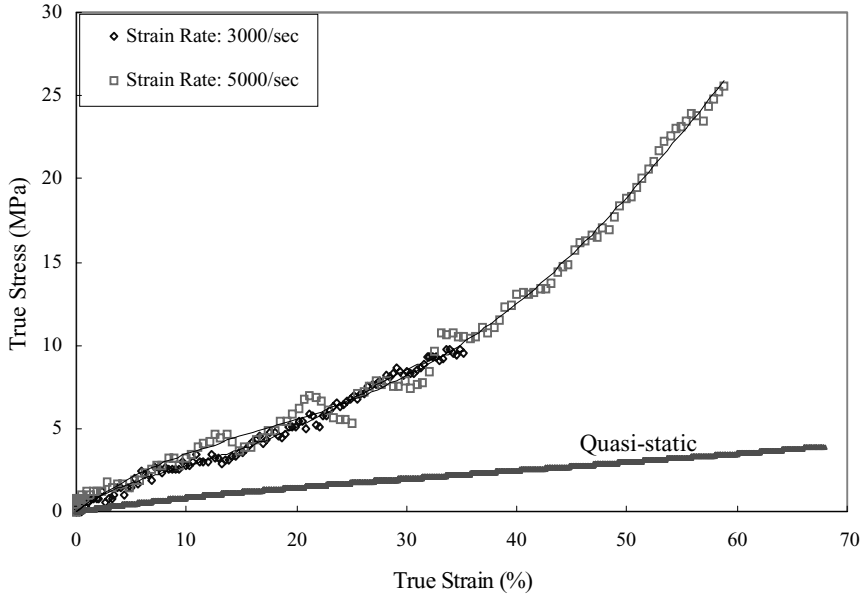

Figure 17 True stress-strain behavior as a function of strain rate for 100% polyurethane.

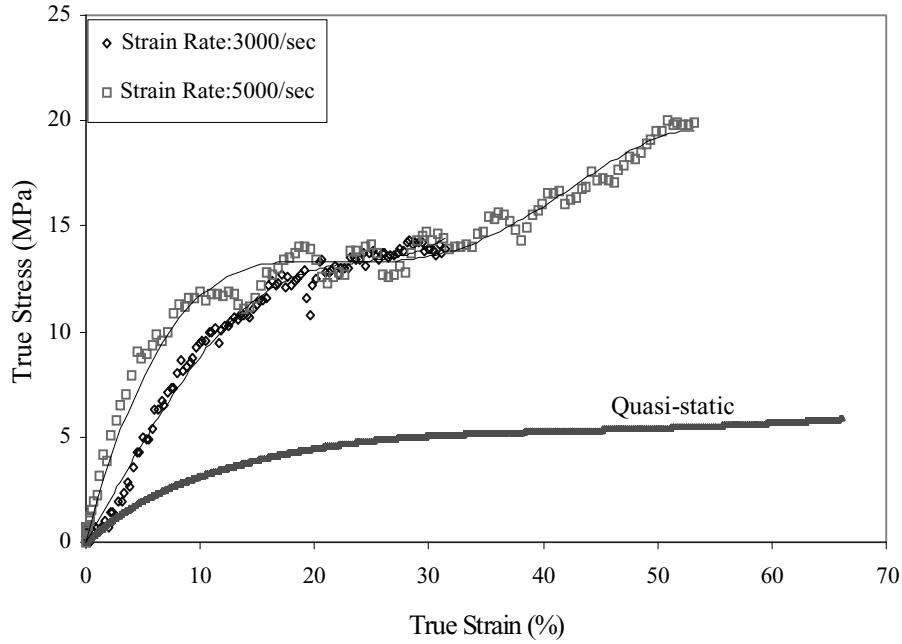

Figure 18 True stress-strain behavior as a function of strain rate for composite of 40% volume fraction of cenospheres.

It is important to point out that the oscillations in stress-strain responses are due to the presence of high frequency components in the strain pulses obtained from the Split Hopkinson Pressure Bar technique. Young's modulus and any other quantities were not measured from these graphs. Simply a qualitative comparison of dynamic constitutive behavior as a function of volume fraction has been performed.

5.2.2. Real-time deformations of high-speed imaging system

It is important to ensure that the specimen undergoes homogeneous deformation during high strain rate loading especially when testing soft materials like polyurethane, which has a high impedance mismatch with the aluminum bars. Tapering of the specimen indicates non-homogeneous state of deformation [9]. The deformation of the specimen was recorded in real-time using the Imacon-200 high-speed camera. The real-time deformation of a specimen, having 20% volume fraction of cenospheres, is shown in Fig. 19. In the second frame (10 μs) the stress wave has just started loading the specimen. Some tapering of the specimen can be observed in the third and fourth frames because the stress wave takes at least two reverberations within the specimen before an equilibrium stress state is achieved. The specimen achieves almost uniform deformation in frame no. 5, i.e., after 40 μs. It can be observed from the rest of the frames that deformation remains uniform throughout the process of dynamic loading. Such homogeneous deformation of the specimen also indicates an equilibrium stress state in the specimen. Similar observations of uniform deformation were made for composites of all volume fractions. Slight barreling of the specimen due to the frictional effects between the

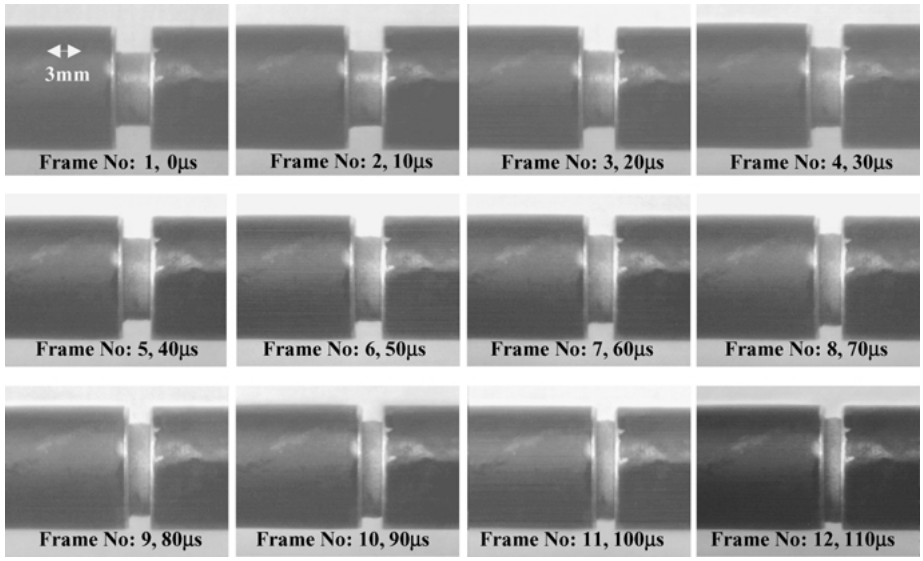

Figure 19 Photograph of real time deformation of polyurethane-cenosphere composite specimen under dynamic loading.

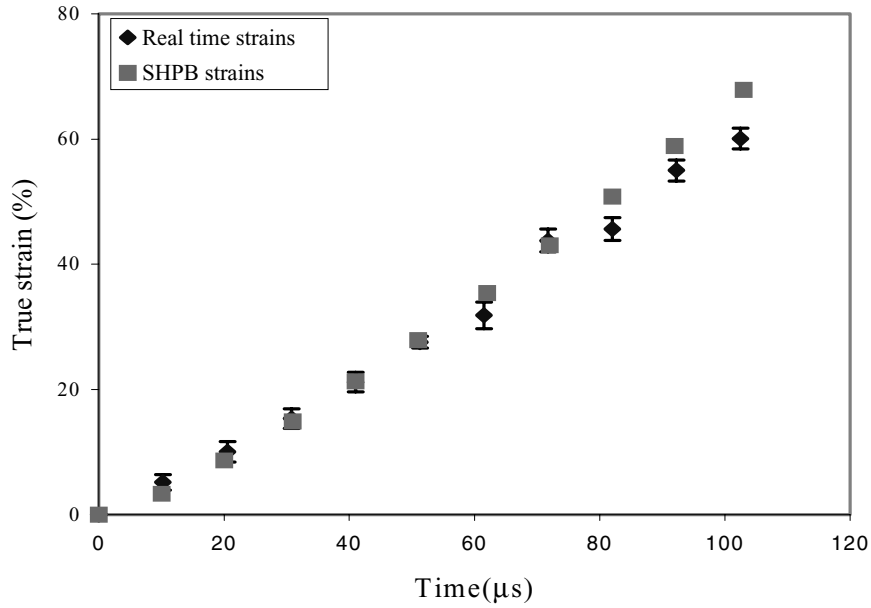

Figure 20 Plot of axial strains obtained from high-speed camera and SHPB.

specimen surface and bars can also be noticed in frames 9 to 12. In spite of applying sufficient lubricant barreling of the specimen could not be eliminated completely. Since the real time deformations are available from the photographs, true strains in the specimen were determined from them using the image analysis software of the high-speed imaging system. A comparison of the true strains obtained from high-speed imaging and SHPB is shown in Fig. 20. It can be observed from the plot that the real-time strains obtained from the high-speed camera match well with the SHPB strains.

6. Conclusions

A simple fabrication procedure to make consistent quality polyurethane-cenosphere particulate composite material was established and a detailed quasi-static and dynamic characterization of the composites was performed. The results of the characterization indicate the following:

- Addition of cenospheres decreases the mass density of the composite. Adding 40% by volume of cenospheres reduces the density by 20%.
- The quasi-static Young's modulus both in tension and compression increases by 400% as the volume fraction of the cenospheres increases to 40%.
- Quasi-static tensile strength increases up to 20% volume fraction of the cenospheres and decreases with further addition of cenospheres. However, the specific tensile strength of the composite is more than that of polyurethane for all volume fractions. The tensile percentage elongation at break decreases from 60% to 10% as the volume fraction of cenospheres is increased to 40%.
- Addition of 40% volume fraction of cenospheres increases the quasi-static fracture toughness of the composite by 100%.
- A predictive model to estimate the composite fracture toughness was developed. The estimates of fracture toughness using this model match well

with experimental results up to a cenosphere volume fraction of 20%.

- The dynamic constitutive behavior of the composite in compression was significantly different from the quasi-static response. At higher strain rates polyurethane exhibited monotonic stiffening behavior where as the composite at higher volume fractions exhibited a stiffening-softening-stiffening behavior.

Acknowldgements

The financial support of National Science Foundation (NSF), under grant No. CMS 99000138 is greatly acknowledged.

References

1. U. YILMAZER and R. J. FARRIS, *J. Appl. Polym. Sci.* **28** (1983) 3369.
2. K. CHEHAB and C. L. BEATTY, in Proceedings of the ACS Division of Polymeric Materials (Div. of Polymeric Materials: Science & Engineering, Washington, DC, USA 1987) Vol. 56, p. 449.
3. H. D. ROZMAN, G. S. TAY, A. ABUBAKAR and R. N. KUMAR, *Eur. Polym. J.* **37** (2001) 1759.
4. A. M. TORRO-PALAU, J. C. FERNANDEZ-GARCIA, A. C. ORGILES-BARCELO and J. M. MARTIN-MARTINEZ, *Int. J. Adhes. Adhes.* **21** (2001) 1.
5. SZ. MOLNAR, B. PUKANSZKY, C. O. HAMMER and F. H. J. MAURER, *Polymer* **41** (2000) 1529.
6. R. J. CARDOSO, A. SHUKLA and A. BOSE, *J. Mater. Sci.* **37** (2002) 603.
7. R. P. SINGH, M. ZHANG and D. CHAN, *ibid.* **37** (2002) 781.
8. A. SHARMA, A. SHUKLA and R. A. PROSSER, *ibid.* **37** (2002) 1005.
9. W. CHEN, F. LU, D. J. FREW and M. J. FORRESTAL, *Trans ASME* **69** (2002) 214.
10. T. WANDELL, *Amer. Ceram. Soc. Bull.* **75**(6) (1996) 79.
11. S. PERVEZ, G. S. PANDEY and V. K. JAIN, *Res. Ind.* **38** (1993) 99.
12. R. M. CLAYTON and L. H. BACK, *J. Eng. Gas Turbines Power Trans ASME* **111** (1989) 679.
13. E. GUTH, *J. Appl. Phys.* **16** (1945) 20.
14. J. S. BERGSTRÖM and M. C. BOYCE, *Rubber Chem. Technol.* **72** (1999) 633.
15. M. A. EL-HADEK and H. V. TIPPUR, *J. Mater. Sci.* **37** (2002) 1649.
16. P. K. ROHATGI and R. Q. GUO, in Proceeding of the 59th Annual American Power Conference, 1997 (Illinois Inst of Technology, Chicago, IL, USA) p. 828.
17. T. L. ANDERSON, "Fracture Mechanics" (CRS Press, Washington D.C., 1995) p.61.
18. H. KOLSKY, *Proc. R. Soc. Lond.* B **62** (1949) 676.

Received 11 July
and accepted 9 January 2003